Publ. Astron. Soc. Japan (2018) 70 (SP2), S52 (1–14)
doi: 10.1093/pasj/psy020

Triggering the formation of the supergiant H II region NGC 604 in M 33

Kengo Tachihara,[1,*] Pierre Gratier,[2] Hidetoshi Sano,[1,3] Kisetsu Tsuge,[1] Rie E. Miura,[4] Kazuyuki Muraoka,[5] and Yasuo Fukui[1,3]

[1]Department of Physics, Nagoya University, Furo-cho, Chikusa-ku, Nagoya, Aichi 464-8602, Japan
[2]Laboratoire d'Astrophysique de Bordeaux, Univ. Bordeaux, CNRS, B18N, Allée Geoffroy Saint-Hilaire, 33615 Pessac, France
[3]Institute for Advanced Research, Nagoya University, Furo-cho, Chikusa-ku, Nagoya, Aichi 464-8601, Japan
[4]Chile Observatory, National Astronomical Observatory of Japan, National Institutes of Natural Sciences, 2-21-1 Osawa, Mitaka, Tokyo 181-8588, Japan
[5]Department of Physical Science, Graduate School of Science, Osaka Prefecture University, 1-1 Gakuen-cho, Naka-ku, Sakai, Osaka 599-8531, Japan

*E-mail: k.tachihara@a.phys.nagoya-u.ac.jp

Received 2017 December 28; Accepted 2018 February 6

Abstract

Formation mechanism of a supergiant H II region NGC 604 is discussed in terms of collision of H I clouds in M 33. An analysis of the archival H I data obtained with the Very Large Array (VLA) reveals complex velocity distributions around NGC 604. The H I clouds are composed of two velocity components separated by $\sim$20 km s^{-1} for an extent of $\sim$700 pc, beyond the size of the the H II region. Although the H I clouds are not easily separated in velocity with some mixed component represented by merged line profiles, the atomic gas mass amounts to 6×10^6 $M_\odot$ and 9×10^6 $M_\odot$ for each component. These characteristics of H I gas and the distributions of dense molecular gas in the overlapping regions of the two velocity components suggest that the formation of giant molecular clouds and the following massive cluster formation have been induced by the collision of H I clouds with different velocities. Referring to the existence of a gas bridging feature connecting M 33 with M 31 reported by large-scale H I surveys, the disturbed atomic gas possibly represents the result of past tidal interaction between the two galaxies, which is analogous to the formation of the R 136 cluster in the LMC.

Key words: ISM: clouds — ISM: individual objects (M 33, NGC 604) — radio lines: ISM — stars: formation

1 Introduction

Dynamical interactions of galaxies are believed to be a major driver of active star formation. Large-scale galaxy collisions or mergers make active starbursts happen, and accelerate the galaxy evolution and metal enrichment (e.g., Genzel et al. 1998). It is widely believed that galaxies evolve as they undergo collisions to merge with other galaxies. Physical processes of the massive cluster formation has not been well understood in detail yet as they are not spatially resolved due to their large distances. The Milky Way Galaxy should also have experienced such dynamical events in the past although the current star formation activity is not as

high as is observed in starburst galaxies. The existence of globular clusters in the Galactic halo suggests past starburst activities, and hence, investigation of the formation of rich star clusters is a key to understanding the evolution history of the Galaxy.

Close encounters of galaxies, on the other hand, as a small-scale interaction between galaxies is supposed to disturb materials in galaxies and enhance the star formation activity (e.g., Noguchi & Ishibashi 1986). The tidal force acting between two galaxies during the encounter strips off a portion of the interstellar material, and that material may fall back down on to the galaxies after the encounter. The Magellanic system is suggested as an example of such events, proposed theoretically by Fujimoto and Sofue (1976), Fujimoto and Noguchi (1990), and represented via numerical simulations by Bekki and Chiba (2007a, 2007b). These simulations show that the two Magellanic clouds had close encounters about 2×10^8 yr ago and streaming H I gas is falling down on to the disk of the Large Magellanic Cloud (LMC) with a velocity of $\sim$50 km s^{-1}. Most recently, Fukui et al. (2017) suggested that the super-star cluster RMC 136 (hereafter R 136) has been formed by the triggering of colliding H I flow falling from the Small Magellanic Cloud (SMC) to the LMC.

M 33 is a member of the local galaxy group associated with M 31, and harbors NGC 604, which is a super-star cluster system similar to R 136. H I high-velocity clouds (HVCs) in the proximity of M 33 have been discovered, and possible origins have been discussed (Grossi et al. 2008). Among them, gas fueling from M 31 seems to be reasonable since the bridge of H I gas, called the M 31–M 33 stream, is detected by the Westerbork Sythesis Radio Telescope (WSRT) (Braun & Thilker 2004), the Arecibo radio telescope (Putman et al. 2009), and the Green Bank Telescope (GBT) (Lockman et al. 2012). The M 31–M 33 stream is successfully reproduced by numerical simulations similar to the Magellanic stream (Bekki 2008). These thus form compelling evidence that continuous gas accretion of 0.5 $M_\odot$ yr^{-1} provides necessary fueling for sustaining M 33's relatively active star formation rate (Grossi et al. 2008). This implies that the formation of young super-star cluster NGC 604 in M 33, the largest and brightest H II region next to R 136 among the local group, could be triggered by the H I cloud collision falling down from the stream to the disk, by analogy with R 136.

The NGC 604 cluster, with an age of 3–5 Myr, contains more than 200 O-type stars associated with a bright Hα nebula extending to a radius of 200–400 pc (e.g., Relaño & Kennicutt 2009) at a distance of 794 kpc from the Sun (McConnachie et al. 2004). The stellar mass of NGC 604 amounts to $\sim 4 \times 10^5$ $M_\odot$ (Eldridge & Relaño 2011). The feedback of the expanding H II region and sequential star formation have been discussed with the existence of arc-like Hα nebula, warm molecular gas, and the spatial gradient of the star formation efficiency as the indicators of interaction and triggering of the 2nd generation star formation (Yang et al. 1996; Tenorio-Tagle et al. 2000; Tosaki et al. 2007; Miura et al. 2010). The latter two papers argue that the second-generation star clusters are triggered by the expansion of the H II region excited by the central star cluster. From the evolutional stages of molecular clouds, star formation propagates from the central cluster where molecular and atomic gas has a cavity $\sim$100 pc to the south, where massive giant molecular clouds (GMCs) are distributed. The timescale of this propagation is estimated to be of the order of 10^6 yr, comparable to the cluster age (Tosaki et al. 2007).

In this paper, we focus on the formation mechanism of NGC 604 by investigating the velocity structure of H I gas around it, particularly in terms of triggering. Section 2 describes the archival H I data and data analysis. Section 3 gives the results of multiple velocity decompositions of the H I gas and their distributions. We then discuss the possibility of colliding H I gas that may trigger molecular cloud formation and subsequent massive cluster (NGC 604) formation in section 4, and summarize in section 5.

2 Archival data and data analysis

The whole of M 33 has been surveyed in atomic gas with the Very Large Array (VLA) and in molecular gas with the Nobeyama 45 m and IRAM 30 m telescopes with a spatial resolution better than 20″ (corresponding to 77 pc). This enabled us to identify individual atomic and molecular clouds, and perform statistical studies with their properties, such as star formation activities represented by the association of H II regions.

The H I mosaic data were obtained from the archive of the VLA with the configurations of B, C, and D. They were reduced and imaged by Gratier et al. (2010) on the Common Astronomy Software Applications (CASA). The datasets were merged, and in the *uv* plane with subsequent imaging and deconvolution of the merged dataset the four resolutions of 5″, 12″, 17″, and 25″ were obtained by tapering in the UV plane, with a 1.27 km s^{-1} channel width covering the area of 0.84 deg^2 (see Gratier et al. 2010 for more detail). Those of 12″ (46 pc) resolution oversampled with 4″ pixel scale are used in this paper as the signal-to-noise ratio of the 5″ map is not sufficient compared to the one at 12″. The top panel of figure 1 shows the integrated intensity mosaic map of the H I emission covering the entire star-forming disk of M 33, showing dense atomic gas clouds concentrated along the spiral arms. The bottom panel of figure 1 shows the position–velocity (PV) diagram with the intensity averaged along the declination. Because of the inclination and rotation of the galaxy, the diagram demonstrates

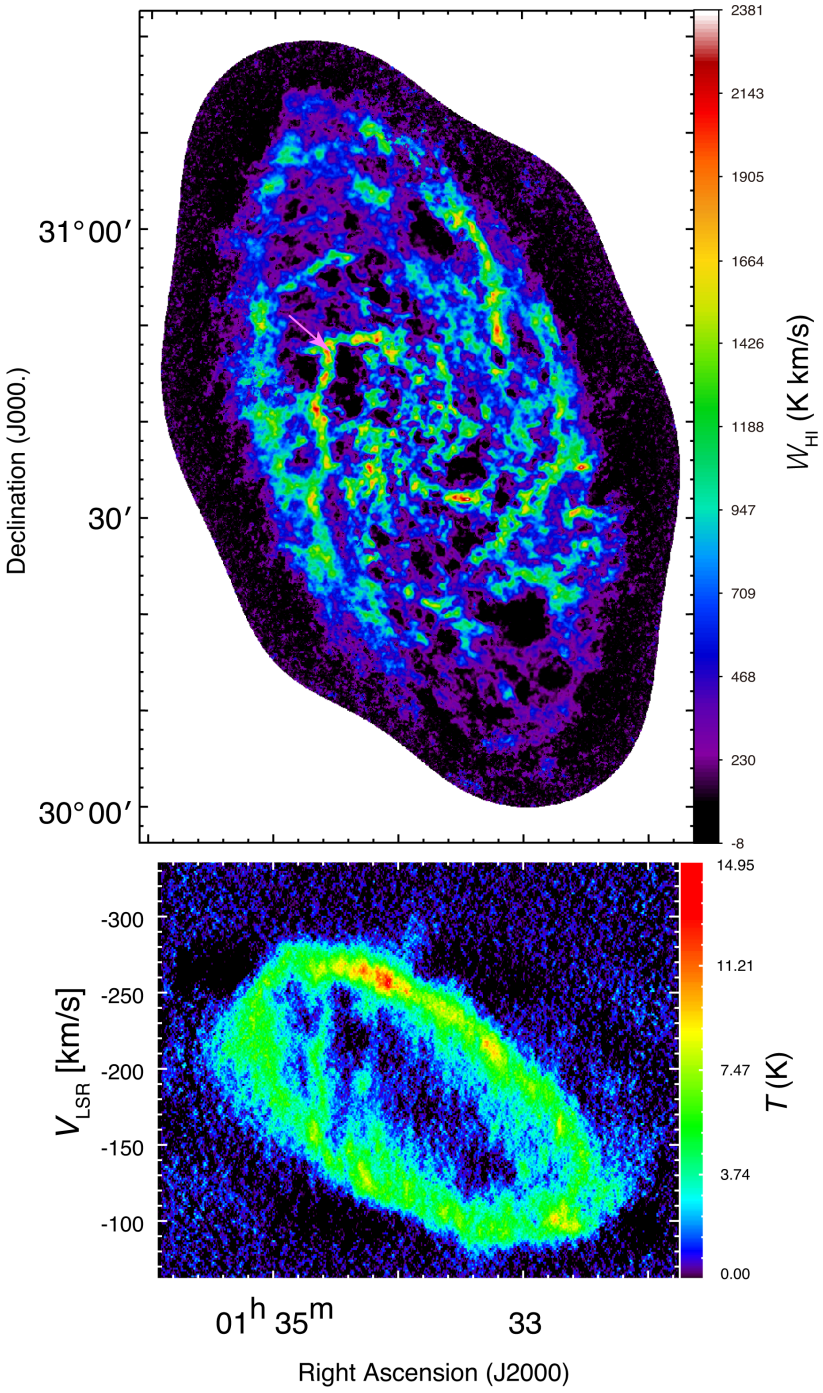

Fig. 1. Top: Integrated intensity map of the VLA H I data for the whole M 33 disk. Bottom: Position–velocity diagram of the H I data averaged over the declination axis. The arrow denotes the position of NGC 604.

elliptical intensity distribution with the spectra blueshifted in the northeast and redshifted in the southwest.

In order to compensate the velocity gradient due to the inclination and galaxy rotation, the spectra at each pixel are shifted assuming that the galaxy has a flat rotation following the model expressed as a tanh function:

$$V(r) = V_\infty \tanh(r/r_0) + V_0, \quad (1)$$

where V_∞ is the circular velocity at $r > r_0$, r_0 is the radius where the velocity field changes from rigid to flat rotation, and V_0 is the systemic velocity. This is basically the same analytical model as that of Corbelli and Schneider (1997), with slightly modified parameters to minimize the velocity dispersion of the averaged spectra. We first define the rotation center and position angle to have a constant velocity centroid along the inclination axis. Then

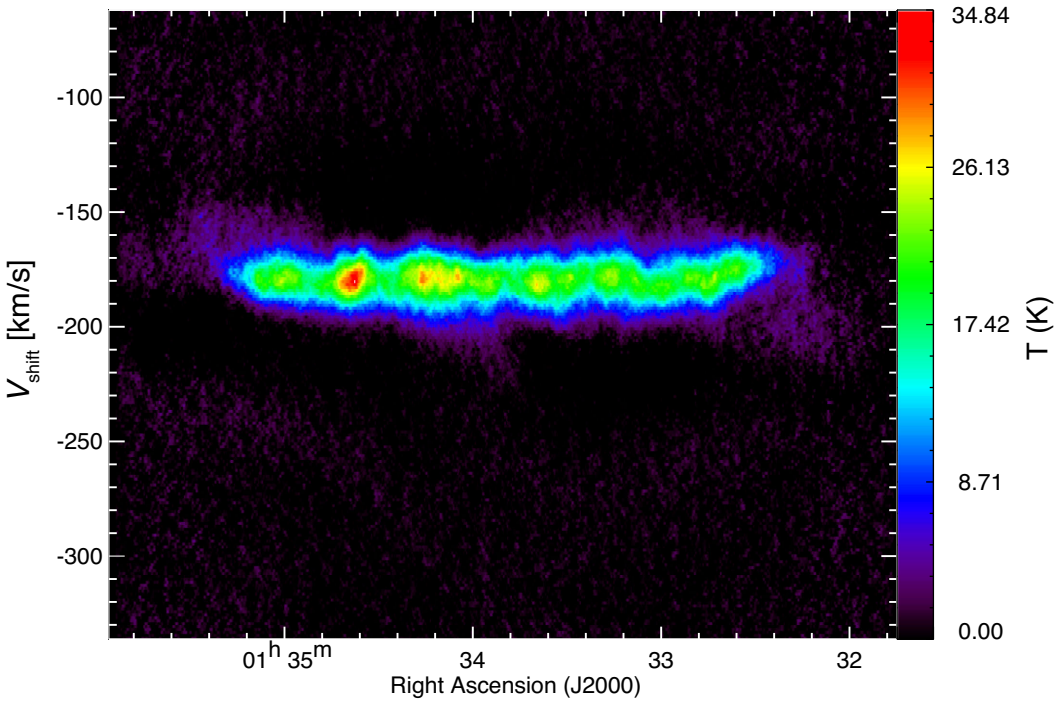

Fig. 2. Position–velocity diagram of the H I data averaged over the declination axis after shifting the velocity reference by the analytical model. The model parameters of the galaxy rotation and inclination are chosen to minimize the velocity gradient.

we search for the best rotation model by changing thes parameters and checking the velocity dispersion of the averaged spectra after applying the velocity shifts. We find that $V_\infty = 107.1\,\mathrm{km\,s^{-1}}$, $r_0 = 8.'27$, and $V_0 = 181.3\,\mathrm{km\,s^{-1}}$ give the best result, while Corbelli and Schneider (1997) estimated a slightly larger value of $r_0 = 8.'47$. The inclination is compensated by the inclination angle $i = 60.°0$, the rotation center at $(\mathrm{RA, Dec})_{\mathrm{J2000.0}} = (1^\mathrm{h}33^\mathrm{m}51.^\mathrm{s}0, +30°39'35'')$, and the position angle $\alpha = 21.°0$. Our best-fitting results give slightly larger i and smaller α, by a few degrees, than previous values given by Regan and Vogel (1994) and Paturel et al. (2003). After compensating the inclination and rotation, the velocity structure is "flattened", as shown in the PV diagram of figure 2. The full-width half maximum (FWHM) of the averaged spectra of thus-shifted data is estimated to be $22.2\,\mathrm{km\,s^{-1}}$. In the following analysis, we use the H I spectra in the thus-shifted velocity frame V_{shift}.

3 Results

3.1 H I clouds around NGC 604

Here we focus on spatial and velocity distributions of the H I clouds around the supergiant H II region NGC 604. Figure 3 shows the detailed cloud distributions superposed on the optically visible nebulosity of NGC 604 imaged by the Hubble Space Telescope (HST). The H I intensity has a depression seen as a cavity where interstellar gas is ionized by the strong UV radiation, and the central cluster is visible through the cavity (see the schematic view of Tosaki et al. 2007). The H I clouds associated with the spiral arm in this part of M 33 has a bent shape with an east–west elongated feature connected with a north–south feature toward NGC 604. It is also connected with a feature of short extension stretched away from the NGC 604 cluster by ∼700 pc to the east. Figure 4 is the velocity channel map of the H I data around NGC 604. As seen in these maps and the PV diagram of figure 5, the clouds of north–south and east–west features associated with the spiral arm are mainly distributed in the velocity range of $-185 < V_{\mathrm{shift}} < -158\,\mathrm{km\,s^{-1}}$, whereas the clouds in the extension feature are relatively blueshifted as $-197 < V_{\mathrm{shift}} < -170\,\mathrm{km\,s^{-1}}$. They both have, however, complex spatial and velocity distributions, and it is difficult to separate them simply by a threshold velocity.

Figure 6 is an H I profile map around NGC 604 with the spatial resolution of 20″ (after 25 pixel binning) and 40″ separation. As clearly seen in the velocity distribution and the double-peaked spectral shapes, the H I gas consists of at least two discrete velocity components. The blueshifted component is dominated by the emission at the velocity of $V_{\mathrm{shift}} \sim -185\,\mathrm{km\,s^{-1}}$, while the redshifted one is at $V_{\mathrm{shift}} \sim -165\,\mathrm{km\,s^{-1}}$, although the entire cloud has complex velocity distribution, with spectra on intermediate velocity

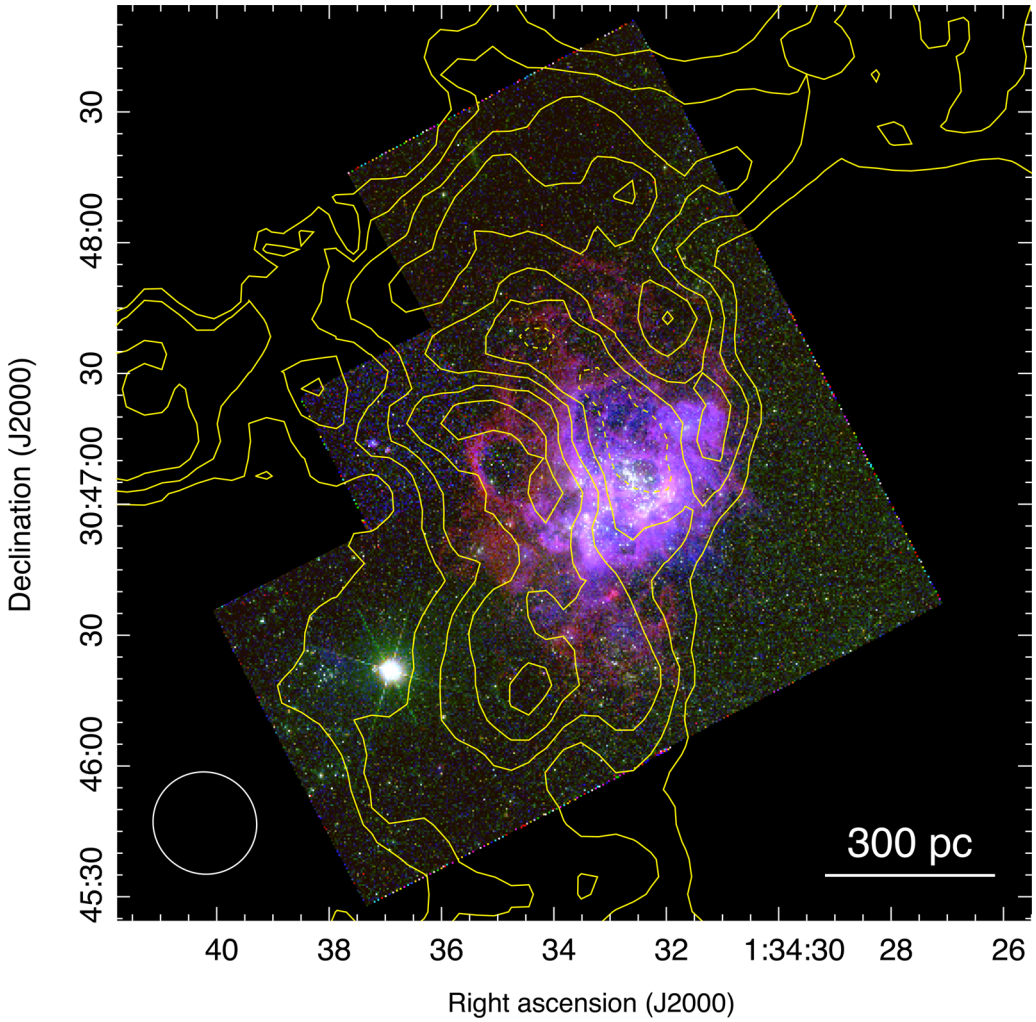

Fig. 3. Composite image of NGC 604 taken with the HST Wide-Field Planetary Camera 2. The red, green, and blue colors represent the images of *F673N*, *F547M*, and *F502N* filter bands, respectively. Overlaid are the contours of the H I line integrated intensity starting from 800 K km s^{-1} with steps of 300 K km s^{-1}. The contours of broken lines denote that the intensities inside of them are depressed. The open circle in the bottom left-hand corner illustrates the synthesized beam size of 12″.

and merged spectra at some positions. The background colors of cyan and magenta denote that the H I spectra is dominated by blue- and redshifted components, respectively, with single-peak velocity close to -185 km s^{-1} and -165 km s^{-1}, respectively. A purple background, on the other hand, shows that the spectra imply the existence of mixed H I gas, as represented by a double-peaked profile or a single-peaked one with a peak velocity of intermediate value.

Note that the clouds in the extended part are dominated with the blueshifted gas, whereas the redshifted component is strong in the western parts of the clouds. The spectra within the NGC 604 H II region, delineated by the blue ellipse in figure 6, have a relatively large velocity dispersion, where the double-peaked profiles are clearly detected outside the ellipse, implying that the complex velocity structure is not only due to the feedback effect of the central cluster, but also the large-scale gas merging of the two velocity components.

3.2 Two-component Gaussian decomposition

In order to characterize physical properties of the H I clouds around NGC 604, decomposition of the spectra by two-component Gaussian fittings are attempted. For the spectrum at each pixel, least-squares regression fittings are adapted with the two-component Gaussian functions. The initial values of the central velocity for the fittings are given as $V_{\rm shift} = -185$ km s^{-1} and -165 km s^{-1}, and the peak intensities and velocity dispersions are set as free parameters. After the iterations, the result of the fitting for each pixel is evaluated, and in case the fitting

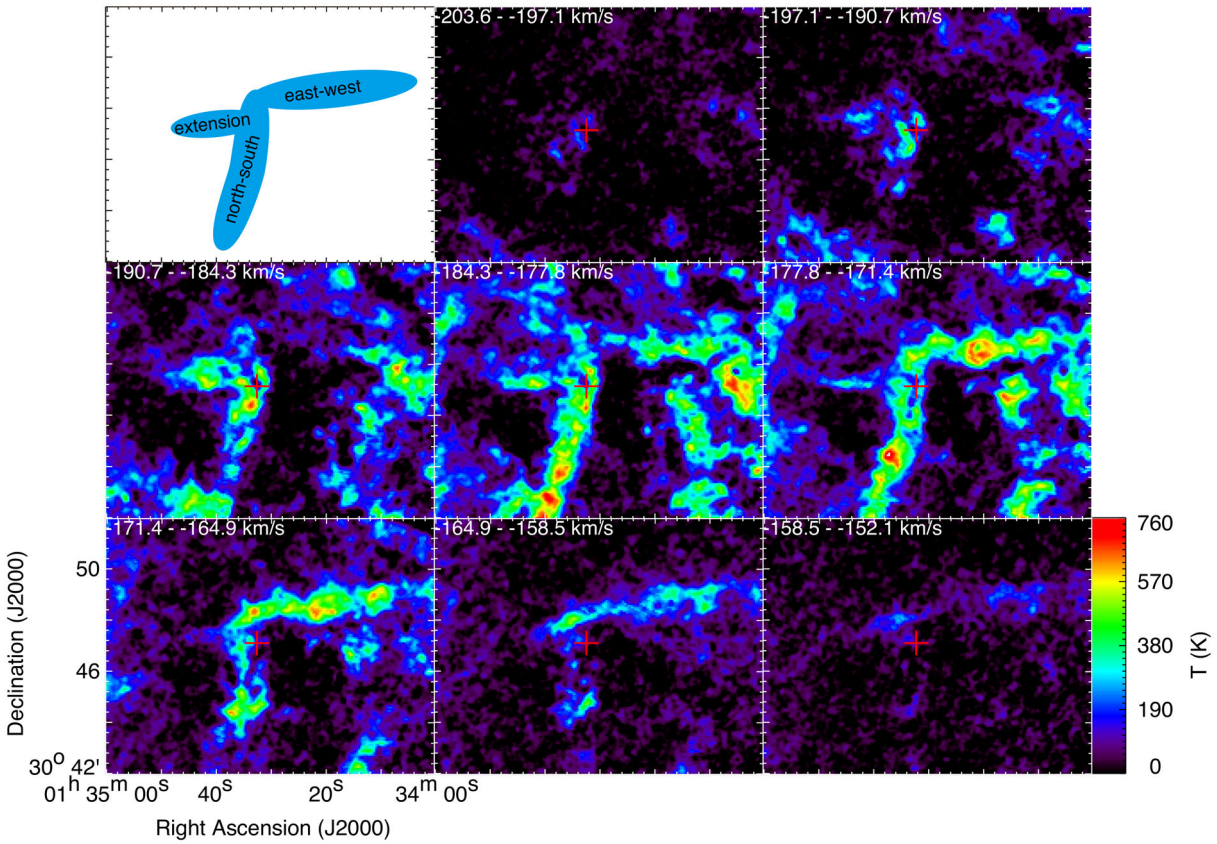

Fig. 4. Velocity channel maps of the clouds around NGC 604 and the associated arm in the shifted velocity frame, $V_{\rm shift}$. Each map exhibits distributions of the integrated intensity of the H I emission over the shifted velocity with the integration range designated at the top left of each panel. The red cross in each panel denotes the position of NGC 604. The top left-hand panel schematically illustrates the positions of the east–west and north–south features and the extension.

failed, fitting is repeated with the single-component Gaussian function. Figure 7 exhibits the distributions of the two separated velocity components with the $-165\,{\rm km\,s^{-1}}$ (redshifted) component as the image and the $-185\,{\rm km\,s^{-1}}$ (blueshifted) one as the contours. Note that when the spectrum is blended, the fitted single-component Gaussian is attributed to the redshifted component, and the gray shaded area denotes the pixels where two-component Gaussian fittings failed. The median values of the resultant central velocity for the red- and blueshifted components are $-165.91\,{\rm km\,s^{-1}}$ and $-183.57\,{\rm km\,s^{-1}}$, respectively. The redshifted component is distributed mainly along the arm, while the blueshifted component spreads from the extension to the region near NGC 604 and also further down to the south along the arm. Towards the central cluster of NGC 604 H II region, both of the velocity components exhibit a depression. Along the arm between $+30^\circ43'30'' <$ Dec $< +30^\circ45'30''$, the H I cloud (hereafter the southern cloud) consists of the two velocity components, while they are mixed at the middle part (Dec $\approx +30^\circ44'30''$) of the cloud.

The H I column density and total mass of the thus-separated components are derived. The column density of H I, $N_{\rm H\,I}$, is calculated from the radiative transfer equation, with the integrated intensity of H I, $W_{\rm H\,I}$, for each pixel assuming the optically thin condition, as:

$$N_{\rm H\,I} = 1.823 \times 10^{18}\, W_{\rm H\,I} \qquad [{\rm cm^{-2}}]\,, \tag{2}$$

where $W_{\rm H\,I}$ is the integrated intensity of the H I emission line, given as $W_{\rm H\,I} = \int T_{\rm b} dv$ with $T_{\rm b}$ representing the observed H I brightness temperature. The blueshifted cloud has a peak column density of $N_{\rm H\,I} = 2.3 \times 10^{21}\,{\rm cm^{-2}}$ at (RA, Dec)$_{\rm J2000.0} = (1^{\rm h}34^{\rm m}41\overset{\rm s}{.}3,\ +30^\circ47'14'')$ for the extension, and $N_{\rm H\,I} = 2.7 \times 10^{21}\,{\rm cm^{-2}}$ at $(1^{\rm h}34^{\rm m}35\overset{\rm s}{.}0,\ +30^\circ45'2'')$ for the southern cloud. The atomic total mass of the blueshifted clouds is estimated by summing up the column density of each pixel, giving $6 \times 10^6\,M_\odot$. The redshifted cloud has, on the other hand, a peak column density of $N_{\rm H\,I} = 3.4 \times 10^{21}\,{\rm cm^{-2}}$ near the border of the NGC 604 H II region. The atomic total mass of the redshifted clouds is $9 \times 10^6\,M_\odot$.

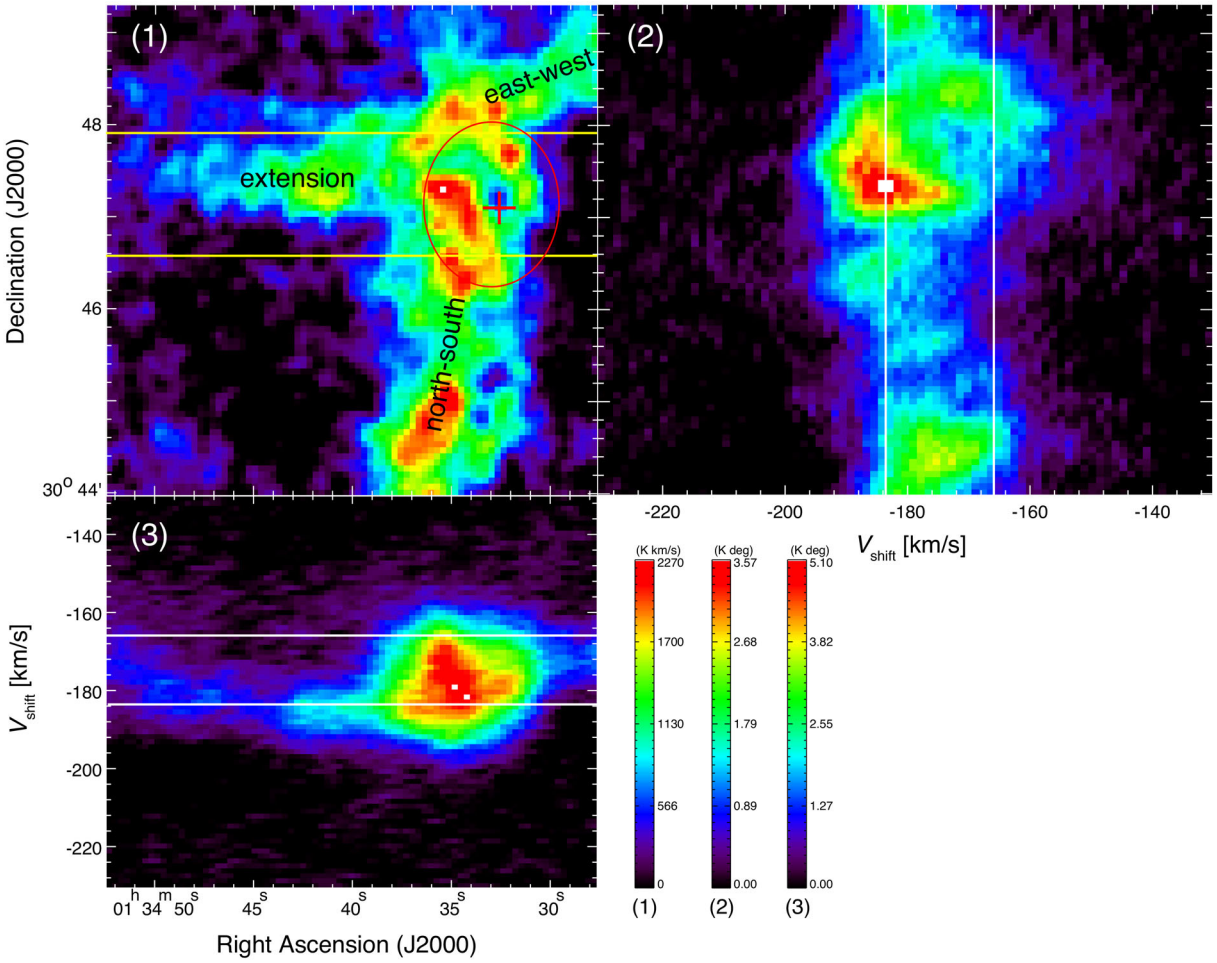

Fig. 5. Zoomed-in image of the H I integrated intensity map around NGC 604 (1), together with the position–velocity diagrams averaged over right ascension (2) and declination (3). The spectra are shifted in velocity to flattened velocity gradient (see text for detail). The red cross denotes the position of NGC 604, with the extent of the surrounding H II region delineated by the red circle. The three color bars for each panel are shown on the bottom right. The two yellow horizontal lines in panel (1) show the integrated range in declination around the cavity for figure 8. The white lines in (2) and (3) designate the median velocities of the red- and blueshifted components (see subsection 3.2).

3.3 Associated CO clouds and their star formation activities

Tosaki et al. (2011) surveyed the entire disk of M 33 for molecular clouds in CO $J = 1$–0 emission with the Nobeyama 45 m telescope, and revealed the molecular fraction $f_{\rm mol}$ distribution as a function of the radial distance from the galactic center. The azimuthally averaged distribution demonstrates a trend of higher $f_{\rm mol}$ for the inner 1.5 kpc region with a peak value of $\sim$0.2, while the outer part has a typical $f_{\rm mol}$ of $\lesssim 0.04$. They suggest a higher metallicity for the inner part of the galaxy. This molecular fraction is given by a ratio of molecular and atomic surface densities, $f_{\rm mol} = \Sigma_{\rm H_2}/(\Sigma_{\rm H\,I} + \Sigma_{\rm H_2})$, and hence is directly comparable to a molecular to atomic mass fraction of $M_{\rm H_2}/(M_{\rm H\,I} + M_{\rm H_2})$ if the molecular and atomic clouds are sampled from the same area. For the clouds in the present region around NGC 604 displayed in figure 7, the total atomic gas mass is estimated by summing up the values of $N_{\rm H\,I}$ and multiplying by the area of the grid and the proton mass to give $M_{\rm H\,I} \sim 1.5 \times 10^7\ M_\odot$, while the molecular cloud mass in the same area is similarly estimated from molecular column density $N_{\rm H_2}$ to be $M_{\rm H_2} = 2 \times 10^6\ M_\odot$ from the CO $J = 1$–0 data, with the assumption of an $X_{\rm CO}$ factor of 3×10^{20} cm^{-2} (K km s^{-1})$^{-1}$ (Wilson & Scoville 1990). This gives an $f_{\rm mol}$ ratio of $\sim$0.12 for the NGC 604 region, significantly higher than the averaged values ($\sim$0.04) estimated for the galactic radius of $\sim$2.8 kpc in M 33 by Tosaki et al. (2011).

On the other hand, Gratier et al. (2012) entirely surveyed the galaxy in the CO ($J = 2$–1) line with the IRAM 30 m telescope and identified 337 GMCs using the CPROPS (Cloud PROPertieS) algorithm (Rosolowsky & Leroy 2006), and compared them with the same dataset of H I as the present work. In the region of our interest around NGC 604, there are GMC #209–#219 and #225. GMC #276 corresponds to

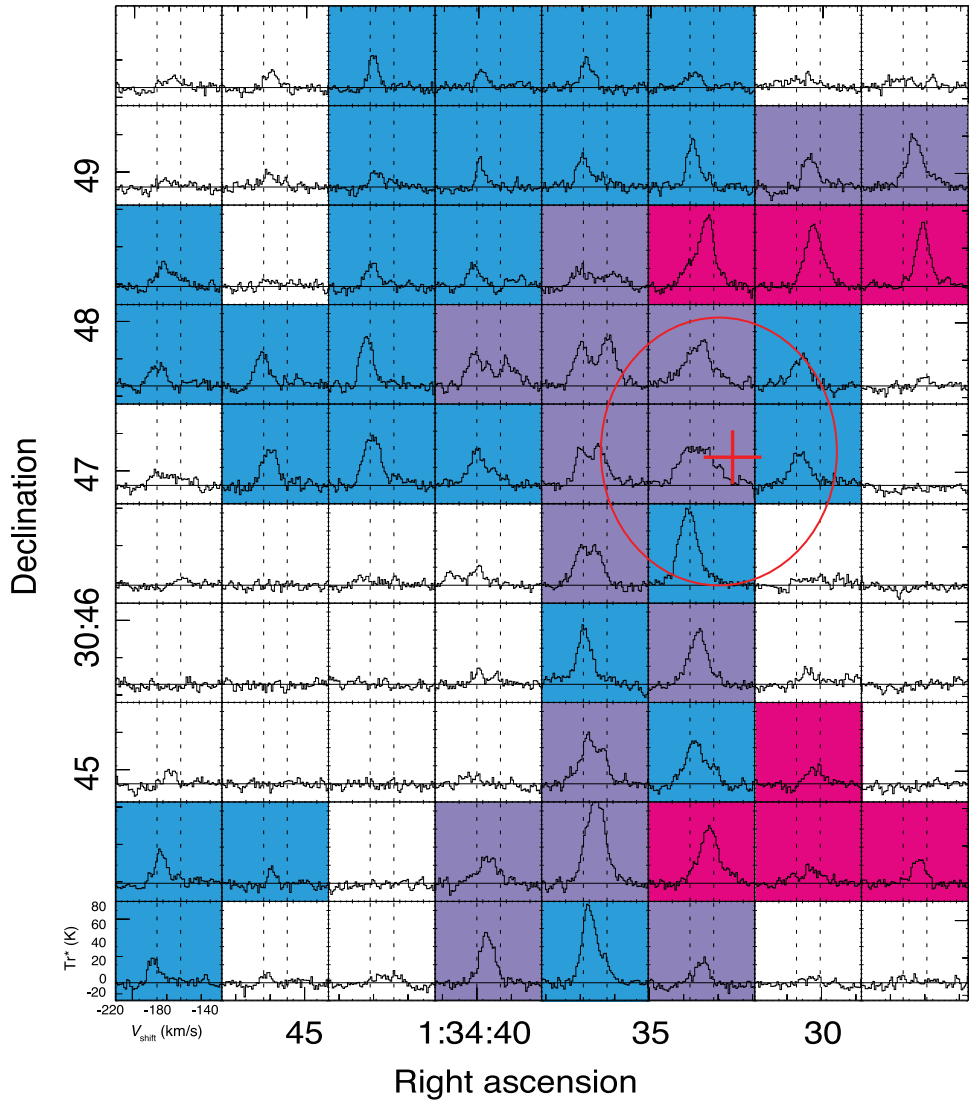

Fig. 6. H I profile map around the NGC 604 region. The spectra are shifted in velocity according to the analytic model (see text), and spatially rebinned down to 20″, and shown in a grid separation of 40″. The red cross denotes the position of NGC 604, with the extent of the surrounding H II region delineated by the red circle. The two dotted lines denote $V_{\rm shift} = -185$ and $-165\,{\rm km\,s^{-1}}$, the initial values of the central velocities for the Gaussian fittings. The background colors of cyan and magenta denote whether the spectra are dominated by blue- and redshifted single component, respectively, while that of purple denotes that spectra are clearly double-peaked, or single-peaked with intermediate peak velocity.

the peak of the blueshifted clouds in the extension feature, while GMC #225 corresponds to the blueshifted peak of the southern cloud. In and around the area of the NGC 604 H II region, several GMCs are distributed (figure 7).

Gratier et al. (2012) classified the GMCs into three types according to their star formation activities, i.e., type A clouds are non-star-forming clouds without any indication of associated stars, type B clouds have embedded star formation with 8 and 24 μm emission but are not seen in Hα or FUV, and type C clouds have exposed star formation with detections in all these bands, in a similar manner to Fukui et al. (1999) and Kawamura et al. (2009) for those in the LMC. This classification is made by several testers independently, and for some GMCs the judgement is not necessarily unique but have large diversities. However, such majority classification gives an idea of star formation activities of the clouds. The CO emission of GMC #276 has a peak velocity corresponding to the blueshifted H I component and is classified as type C. GMCs #225 and #216 also belong to the blueshifted clouds and the major classifications are type C, while another blueshifted GMC, #212, is classified as type A. In addition, GMC #209 is a redshifted type A cloud, and GMC #211 a redshifted type C cloud. GMCs #210 and #218 have double-peaked CO profiles and are classified as type A or B. GMC #213 (type B/C), #214 (type A), #215 (type C), and #217 (type B) have H I and CO lines of blended velocity components. Both the blue- and redshifted clouds have a variety of properties in star

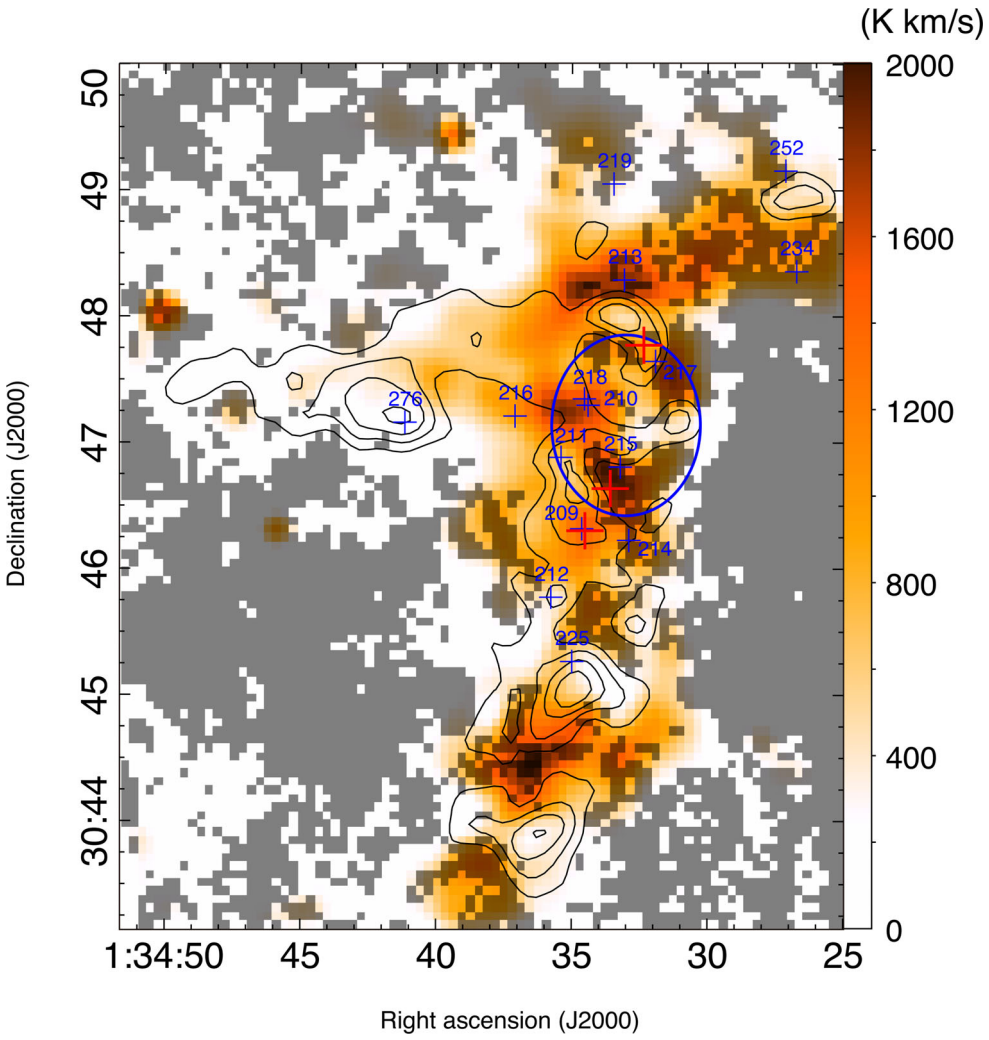

Fig. 7. This image represents the total intensity of the redshifted ($V_{\rm shift} \approx -165\,{\rm km\,s^{-1}}$) H I component derived from the Gaussian fitting, while the overlaid contours are that of the blueshifted ($V_{\rm shift} \approx -185\,{\rm km\,s^{-1}}$) component. The intensity is calculated from the area of the fitted Gaussian function. The image and contours are smoothed by 3 pixel Gaussian filters. The contour levels are from $500\,{\rm K\,km\,s^{-1}}$ with steps of $250\,{\rm K\,km\,s^{-1}}$. The gray shaded areas denote the pixels where two-component Gaussian fitting fails. The blue ellipse delineates the extent of the optical nebula of NGC 604. The blue crosses mark the positions of GMCs with their numbers identified in CO $J = 2$–1 by Gratier et al. (2012). The red crosses show the peak positions of CO $J = 1$–0 intensity (see text and figure 9.)

formation. There is no clear difference in the star formation trend between the blue- and redshifted components. In the present region, about one quarter (27%) of the clouds are designated as type A. This is a slightly large fraction compared to the statistics of the whole clouds sampled from the entire galaxy (15%).

4 Discussion

4.1 Kinematics of the H I clouds

As shown above, the H I clouds around NGC 604 have complex velocity distributions, and they consist of at least two discrete velocity components. Toward some positions, the spectra appear to be merged, having peak velocity between the two components. We consider the origin of the velocity structures. One possibility is the expanding motion energized by the feedback effect of the super-star cluster NGC 604, which is surrounded by multiple shell-like structures of the Hα nebulosity. Tosaki et al. (2007) and Miura et al. (2010) discussed these phenomena from molecular data by single-dish and interferometric observations, respectively. The CO clouds exhibit indications of interaction with the cluster as high $J = 3$–2/1–0 line ratios ($R_{3-2/1-0}$) along the Hα shell, implying the interaction of the molecular clouds with the expanding H II region. The star formation efficiency (SFE) shows a decreasing trend with distance from the NGC 604 cluster, implying the sequential star formation triggered by the feedback effects. The molecular clouds around NGC 604 have not been reported as

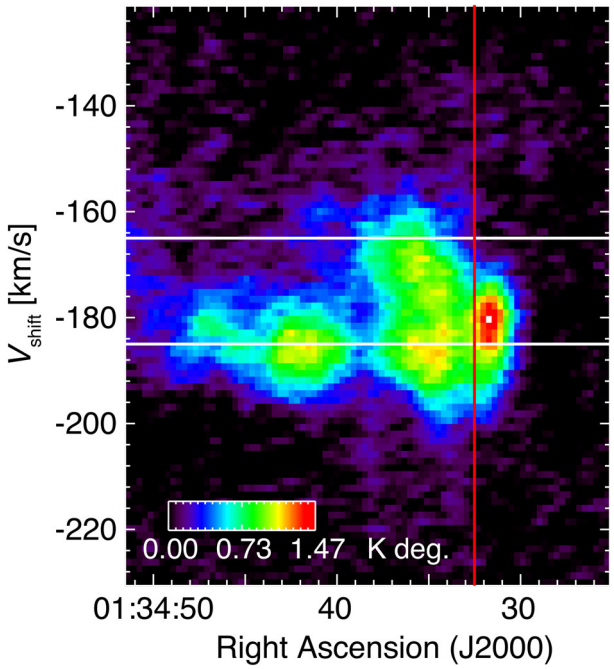

Fig. 8. Position–velocity diagram toward the region including the H I cavity around NGC 604 and the extension cloud. The H I spectra are integrated over the axis of declination for the range between the two white lines in figure 5. The red vertical bar designates the position of H I cavity centered at the NGC 604 super-star cluster, while the horizontal white ones are the median velocities of the decomposed red- and blueshifted components.

exhibiting expanding motion due to the feedback. Figure 8 is the PV diagram focused on the cavity of the H I cloud and the extended cloud to the east (see figure 5). Toward the H I cavity, one can clearly recognize the depression in H I intensity. This is a piece of evidence of feedback from NGC 604 affecting on the H I cloud, likely as photoionization. However, the velocity field does not appear to have a simple expanding motion in this PV diagram. To the west of the cavity (RA $\sim 1^{h}34^{m}32^{s}$), the H I spectra appear to be single-peaked, while those to the east (RA $\sim 1^{h}34^{m}35^{s}$) are multi-peaked (with blue- and redshifted components) or have large velocity dispersions. The eastern cloud extension has blueshifted velocity and is connected to the blueshifted component around the H I cavity. In addition, the distributions of the two velocity components have much larger extents than the Hα nebulosity. If we make a simple assumption that the blue- and redshifted H I clouds are due to the expanding motion with a velocity of 10 km s^{-1}, the kinetic energy of the clouds are estimated to be as much as 6×10^{51} erg. We thus conclude that the feedback effect of NGC 604 on the complex velocity structures of the H I clouds is only limited for a small surrounding area. If we consider kinetic energy injection by supernovae (SNe) explosions with ~5% efficiency (Kruijssen 2012), it requires ~100 SNe within the age of the NGC 604 cluster. The number is still much larger than that expected from the cluster scale. On the other hand, significant energy of radiation that may affect the kinematics of the surrounding interstellar medium is released from the massive stars. It is suggested that the radiation pressure evacuates the interstellar medium from the galactic disk as galactic winds if the cluster mass is more than $\sim 10^{6}\ M_{\odot}$, while the bubble radius is limited to be less than ~30 pc for the cluster mass of $3 \times 10^{5}\ M_{\odot}$ (Murray et al. 2011).

As an alternative possibility to explain the velocity fields, we propose a scenario of gas accretion on to the spiral arm of the disk, which then triggered active star formation of NGC 604. Similar to the case of the Magellanic bridge and the Magellanic stream, the M 31–M 33 system is known to have a diffuse gas bridge connecting the two galaxies (Braun & Thilker 2004; Putman et al. 2009; Lockman et al. 2012). Grossi et al. (2008) detected H I clouds in the proxy of M 33, and suggested that they are HVCs accreting and fueling the M 33 disk for star formation. If this is the case, the formation of NGC 604 is supposed as being triggered by the collision of infalling H I clouds, similar to the case for R 136 in the LMC. The velocity separation between the two components is ~50 km s^{-1} for R 136, about a factor of 2–3 larger than the present case of NGC 604. Bekki (2008) demonstrated by numerical simulations that M 31 and M 33 had a close encounter 4–8 Gyr ago, which resulted in the formation of a gas streamer stretched by tidal force. van der Marel et al. (2012) predicted future encounters and possible mergers of M 31, M 33, and the Milky way in several Gyr. The orbital motion is, however, very complicated and also depends on the assumed initial conditions, particularly at the region close to the galactic disk. It is therefore difficult to predict the relative velocity of the infalling gas with respect to the galactic disk. The blueshifted H I clouds dominating the extension feature is, however, candidate infalling gas from the morphological characteristics. The impact of the collisions between the H I clouds seem to be significant, but the bulk energy of the collision is hard to estimate.

4.2 Formation of molecular gas by shock triggering

Massive molecular clouds are distributed around NGC 604, where active star formation is ongoing. Figure 9 reveals the integrated intensity distribution of CO $J = 1$–0 by contours (Tosaki et al. 2011) overlaid on the H I integrated intensity map. The CO clouds show concentrations in a region around the H I cavity of NGC 604 with clumpy shapes peaked at three positions, denoted by the red crosses. The distributions of the $J = 2$–1 line intensity, on the other hand, are slightly different, namely that GMCs #215 and #217 have peak positions closer to the central cluster of

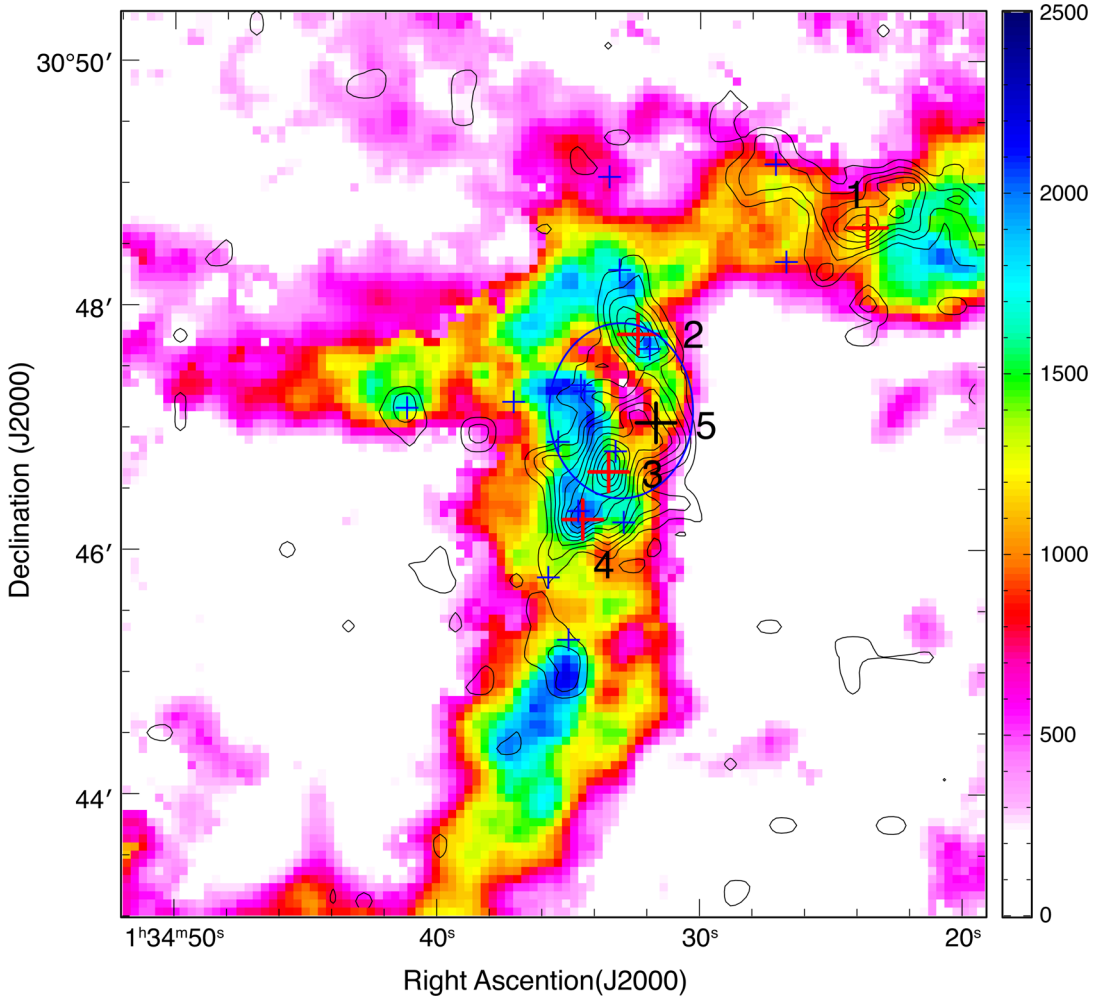

Fig. 9. Integrated intensity map of H I shown by the pseudo-color overlaid with the contours of CO $J = 1$–0 integrated intensity (Tosaki et al. 2007). The crosses denote the positions that have CO and H I spectra displayed in figure 10. The four red crosses correspond to the positions of CO intensity peaks, while the black one represents the NGC 604 cluster. The blue crosses are the positions of GMCs defined in CO $J = 2$–1 by Gratier et al. (2012). The contours are from 0.6 K km s^{-1} with steps of 0.9 K km s^{-1}. The blue ellipse delineates the extent of the optical nebula of NGC 604.

NGC 604 than the $J = 1$–0 peak 2 and peak 3, while the position of peak 4 corresponds well to that of GMC #209 (see figure 7). There is another CO cloud with peak 1 on the east–west feature to the north of NGC 604 (hereafter the "northern cloud"), where H I intensity is depressed in a way that is complementary to the distribution with CO. Figure 10 illustrates the H I and CO spectra sampled at the three peak positions of CO $J = 1$–0 together with those at the H I cavity edge. At peaks 2 and 3, CO emission lines are detected at the intermediate velocity of the two H I components, while at peak 4 the CO line is strong for the redshifted component. The CO clouds are, on the other hand, also detected from the blueshifted component at some positions around the H I cavity, such as position 5. At the position of peak 1, the CO emission has relatively blueshifted velocity with respect to the H I line. These factors imply that not only H I, but also the CO emission, has complex velocity fields.

Figure 11 demonstrates the CO cloud distributions compared with those of the red- and blueshifted H I clouds represented by the contours with integrated velocity ranges of $-214 < V_{\rm shift} < -184$ km s^{-1} and $-175 < V_{\rm shift} < -143$ km s^{-1}, respectively. The CO emission is detected towards the region where the blue and red components are overlapping around NGC 604 and in the southern cloud. The northern cloud, on the other hand, does not have strong blueshifted H I emission in this velocity range, but the Gaussian decomposition succeeded in separating the blueshifted component near GMC #252 (see figure 7).

As discussed above, it is suggested that the two velocity components of the H I clouds seem to be due to the gas

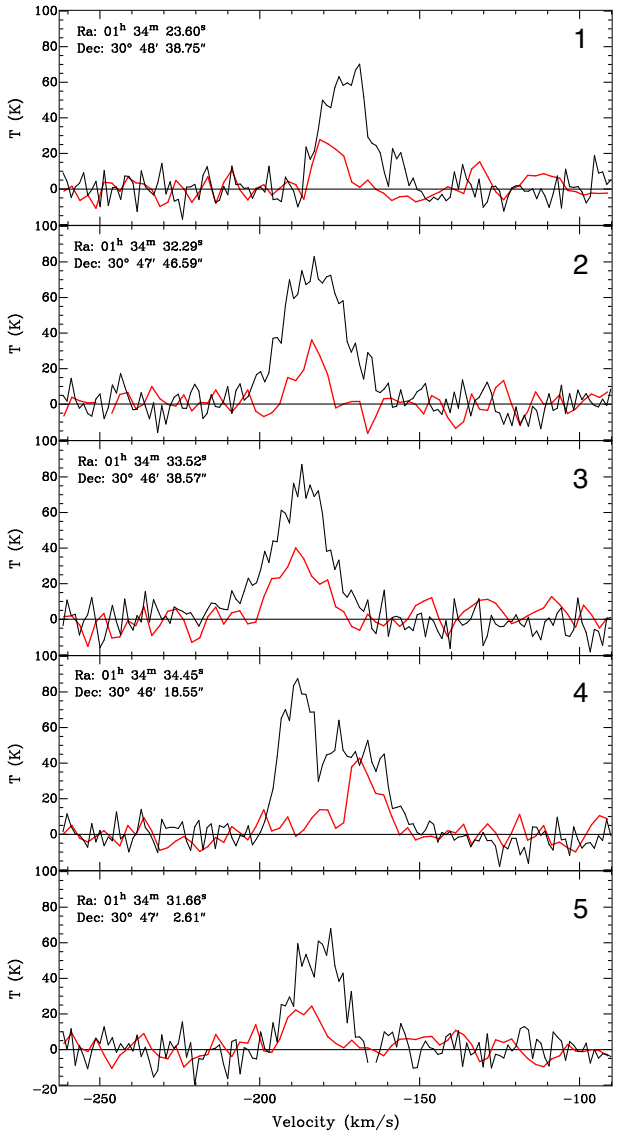

Fig. 10. H I (black) and CO (red) spectra at the five positions shown in figure 9. The CO spectra are scaled by a factor of 5.

infall originating from the tidal interaction between M 31 and M 33, and the collision of the H I clouds triggered the formation of the NGC 604 super-star cluster. If this is the case, the idea of molecular cloud formation by the cloud–cloud collision should be significant. Numerical simulations of colliding gas flow and subsequent thermal instabilities have been investigated by many authors (Field et al. 1969; Wolfire et al. 1995; Koyama & Inutsuka 2000, 2002; Hennebelle et al. 2007; Inoue & Inutsuka 2012).

The dynamical crossing time of the two H I clouds can be calculated from the size of the clouds divided by the relative collision velocity. If we assume the size of the colliding system to be ∼600 pc and a collision velocity of ∼20 km s^{-1}, the resulting crossing time is $\sim 3 \times 10^7$ yr. Within this period, molecular gas formation is feasible if the density is high enough (Goldsmith et al. 2007). Therefore it is suggested that collisions of H I clouds could enhance the local molecular fraction of the interstellar gas, and accelerate the chemical evolution of the galaxy. The local enhancement of $f_{\rm mol} \sim 0.12$ derived above could be affected by ionization of the gas by the UV radiation from the massive star members of NGC 604, namely that the surrounding atomic gas is ionized by the cluster, while the inner molecular clouds are more shielded from the UV irradiation due to the higher column density. The molecular clouds are, however, much more extended beyond the extent of the optically visible H II nebula. The effect of UV ionization seems to be limited, and we hence suggest molecular formation induced by the shock cloud compression triggered by the H I cloud collisions.

4.3 Large-scale gas fueling by M 31–M 33 tidal interaction and triggering of supermassive clusters

As discussed above, the formation of molecular clouds and subsequently NGC 604 are likely to be triggered by collisions of H I clouds. We suggest that such triggering is not an unique phenomenon for NGC 604, but also works for other giant H II regions such as NGC 595, where we see similar double-peaked H I profiles. As suggested by Grossi et al. (2008), continuous mass accretion fuels the galaxy with fresh gas, which maintains active star formation of M 33. They identified H I clouds with high relative velocities in the periphery of M 33, and a blueshifted cloud named AA16 in their catalog is located ∼3 kpc to the east of NGC 604. This might be an indication of gas infall from the galaxy halo or further outside. The origin of the infalling gas is unknown, but the existence of the H I stream between M 31 and M 33 implies tidal interaction betweem them, similar to the formation scenario of the Magellanic stream. Such close encounters of galaxies, or mergers and collisions, are suggested as common triggering phenomena for massive star cluster formation in the evolutional sequence of galaxies.

5 Summary

The H I archival data obtained with VLA has been reanalyzed, and their velocity structures have been investigated, particularly for the region around the super-star cluster NGC 604. The results are summarized below.

- The velocity field of the H I clouds around the super-star cluster NGC 604 appear to have complex structures containing multiple velocity components indicated by double-peaked spectral profiles.

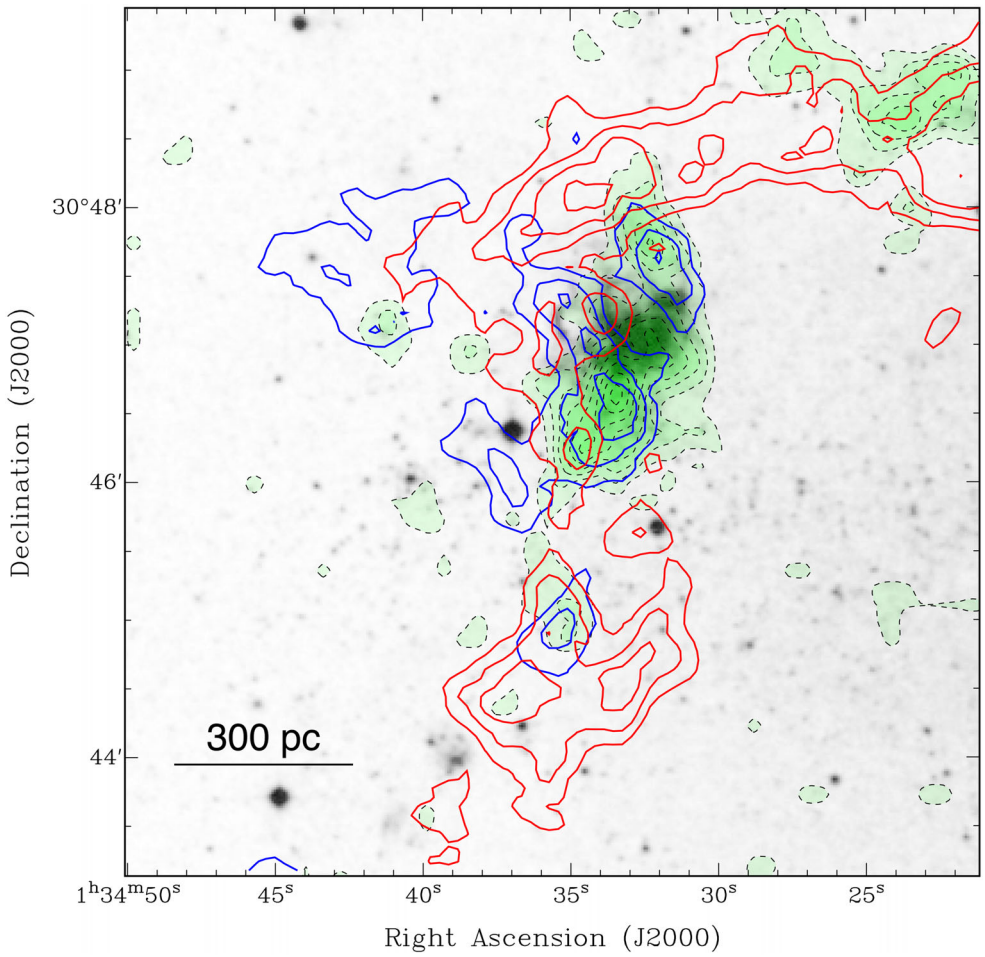

Fig. 11. Distributions of the CO clouds is represented by the green shaded area on top of the optical image of DSS-red in grayscale. Overlaid are the blue and red contours representing the blue- and redshifted H I clouds with the integrated ranges of $-214 < V_{\rm shift} < -184\,{\rm km\,s^{-1}}$ and $-175 < V_{\rm shift} < -143\,{\rm km\,s^{-1}}$, respectively.

- They are decomposed by fittings to the two component Gaussian functions, the central velocities of which are typically separated by 20 km s^{-1}.
- Thus-separated two velocity components are distributed far beyond the extent of the optically visible H II region of NGC 604, and they do not show clear expanding velocity features.
- The atomic gas mass of each blue- and redshifted component is estimated to be $6 \times 10^6\,M_\odot$ and $9 \times 10^6\,M_\odot$, respectively.
- Molecular clouds identified by CO observations are associated with H I clouds of both velocity components, and the CO clouds are mainly distributed towards the overlapped regions of the two velocity H I components.
- It is suggested that the H I clouds are infalling on to the galactic disk and the collision of the clouds induced the molecular cloud formation in $\sim$ a few $\times 10^7$ yr.
- As the mass accretion continued, the collisions of the H I clouds triggered the formation of the super-massive star cluster of NGC 604 several Myr ago.
- As suggested for the formation mechanism of R 136 in the LMC, colliding H I gas originated from the past close encounter and the tidal effect between galaxies can be a major trigger of super-star cluster formation. This is consistent with the galaxy merger paradigm for the galaxy evolution scenario.

Funding

The work is supported by Japan Society for the Promotion of Science (JSPS) KAKENHI Grant Number JP15H05694.

Acknowledgments

Based on observations made with the NASA/ESA Hubble Space Telescope, and obtained from the Hubble Legacy Archive, which is a collaboration between the Space Telescope Science Institute (STScI/NASA), the Space Telescope European Coordinating Facility (ST-ECF/ESA) and the Canadian Astronomy Data Centre (CADC/NRC/CSA). The National Radio Astronomy Observatory is

a facility of the National Science Foundation operated under cooperative agreement by Associated Universities, Inc. The Nobeyama 45 m radio telescope is operated by Nobeyama Radio Observatory, a branch of the National Astronomical Observatory of Japan.

References

Bekki, K. 2008, MNRAS, 390, L24
Bekki, K., & Chiba, M. 2007a, MNRAS, 381, L16
Bekki, K., & Chiba, M. 2007b, PASA, 24, 21
Braun, R., & Thilker, D. A. 2004, A&A, 417, 421
Corbelli, E., & Schneider, S. E. 1997, ApJ, 479, 244
Eldridge, J. J., & Relaño, M. 2011, MNRAS, 411, 235
Field, G. B., Goldsmith, D. W., & Habing, H. J. 1969, ApJ, 155, L149
Fujimoto, M., & Noguchi, M. 1990, PASJ, 42, 505
Fujimoto, M., & Sofue, Y. 1976, A&A, 47, 263
Fukui, Y., et al. 1999, PASJ, 51, 745
Fukui, Y., Tsuge, K., Sano, H., Bekki, K., Yozin, C., Tachihara, K., & Inoue, T. 2017, PASJ, 69, L5
Genzel, R., Lutz, D., & Tacconi, L. 1998, Nature, 395, 859
Goldsmith, P. F., Li, D., & Krčo, M. 2007, ApJ, 654, 273
Gratier, P., et al. 2010, A&A, 522, A3
Gratier, P., et al. 2012, A&A, 542, A108
Grossi, M., Giovanardi, C., Corbelli, E., Giovanelli, R., Haynes, M. P., Martin, A. M., Saintonge, A., & Dowell, J. D. 2008, A&A, 487, 161
Hennebelle, P., Audit, E., & Miville-Deschênes, M.-A. 2007, A&A, 465, 445
Inoue, T., & Inutsuka, S. 2012, ApJ, 759, 35
Kawamura, A., et al. 2009, ApJS, 184, 1
Koyama, H., & Inutsuka, S. 2000, ApJ, 532, 980
Koyama, H., & Inutsuka, S. 2002, ApJ, 564, L97
Kruijssen, J. M. D. 2012, MNRAS, 426, 3008
Lockman, F. J., Free, N. L., & Shields, J. C. 2012, AJ, 144, 52
McConnachie, A. W., Irwin, M. J., Ferguson, A. M. N., Ibata, R. A., Lewis, G. F., & Tanvir, N. 2004, MNRAS, 350, 243
Miura, R., et al. 2010, ApJ, 724, 1120
Murray, N., Ménard, B., & Thompson, T. A. 2011, ApJ, 735, 66
Noguchi, M., & Ishibashi, S. 1986, MNRAS, 219, 305
Paturel, G., Theureau, G., Bottinelli, L., Gouguenheim, L., Coudreau-Durand, N., Hallet, N., & Petit, C. 2003, A&A, 412, 57
Putman, M. E., et al. 2009, ApJ, 703, 1486
Regan, M. W., & Vogel, S. N. 1994, ApJ, 434, 536
Relaño, M., & Kennicutt, R. C., Jr. 2009, ApJ, 699, 1125
Rosolowsky, E., & Leroy, A. 2006, PASP, 118, 590
Tenorio-Tagle, G., Muñoz-Tuñón, C., Pérez, E., Maíz-Apellániz, J., & Medina-Tanco, G. 2000, ApJ, 541, 720
Tosaki, T., et al. 2011, PASJ, 63, 1171
Tosaki, T., Miura, R., Sawada, T., Kuno, N., Nakanishi, K., Kohno, K., Okumura, S. K., & Kawabe, R. 2007, ApJ, 664, L27
van der Marel, R. P., Besla, G., Cox, T. J., Sohn, S. T., & Anderson, J. 2012, ApJ, 753, 9
Wilson, C. D., & Scoville, N. 1990, ApJ, 363, 435
Wolfire, M. G., Hollenbach, D., McKee, C. F., Tielens, A. G. G. M., & Bakes, E. L. O. 1995, ApJ, 443, 152
Yang, H., Chu, Y.-H., Skillman, E. D., & Terlevich, R. 1996, AJ, 112, 146